Stage Separation Failure: Model Based Diagnostics and Prognostics

Dmitry Luchinsky[1], Vasyl Hafiychuk[2], Igor Kulikov[3], Vadim Smelyanskiy[4], Ann Patterson-Hine[5], John Hanson[6], Ashley Hill[7]

[1,2,3,4,5]*NASA Ames Research Center, Mail Stop 269-1, Moffett Field, CA 94035, USA*

Dmitry.G.Luchinsky@nasa.gov
Vasyl.Hafiychuk@nasa.gov
Igor.K.Kulikov@jpl.nasa.gov
Vadim.N.Smelyanskiy@nasa.gov
Ann.Patterson-Hine@nasa.gov

[6,7]NASA Marshall Space Flight Center, Huntsville, Alabama 35812

Ashley.D.Hill@nasa.gov
John.M.Hanson@nasa.gov

ABSTRACT

Safety of the next-generation space flight vehicles requires development of an in-flight Failure Detection and Prognostic (FD&P) system. Development of such system is challenging task that involves analysis of many hard hitting engineering problems across the board. In this paper we report progress in the development of FD&P for the re-contact fault between upper stage nozzle and the inter-stage caused by the first stage and upper stage separation failure. A high-fidelity models and analytical estimations are applied to analyze the following sequence of events: (i) structural dynamics of the nozzle extension during the impact; (ii) structural stability of the deformed nozzle in the presence of the pressure and temperature loads induced by the hot gas flow during engine start up; and (iii) the fault induced thrust changes in the steady burning regime. The diagnostic is based on the measurements of the impact torque. The prognostic is based on the analysis of the correlation between the actuator signal and fault-induced changes in the nozzle structural stability and thrust.[*]

1. INTRODUCTION

Stage separation failure may have various origins including e.g. failure of the accelerating/decelerating motors during the separation. The combined expected failure rate is relatively high and is the second most common cause of launch failures (Futron Corporation, 2004). Despite of this fact a reliable in-flight diagnostic and prognostic system for this fault is currently unavailable. Below we report a progress in development of such system.

We consider two-stage, vertically stacked space vehicle. The vehicle is propelled by the first stage booster at the first phase of the flight. After the rocket booster completes its mission, the stages separate and the second stage engine provides the propulsion during the second phase of the flight. Due to separation faults, the first stage can collide with the second stage engine nozzle and damage it. The hot gas flow may result in further degradation of the nozzle, reduction of the actual thrust, and significant side loads.

Development of an in-flight FD&P system for this fault is a challenging engineering problem (Seife, 2003). The main difficulties stem from the fact that the phenomena underlying fault dynamics are highly non-linear in structural, thermal, and fluid dynamical domains.
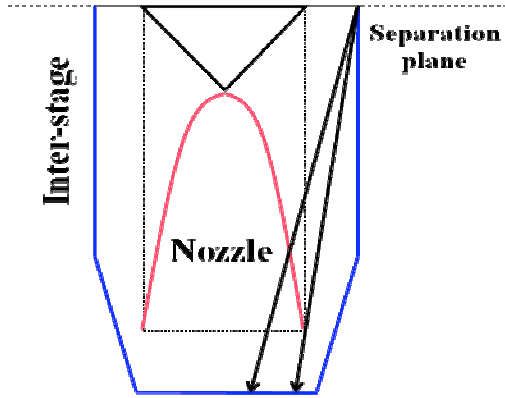
Figure 2 Sketch of the separation failure geometry. Two fault induced separation trajectories are shown by black lines. Left path corresponds to sever impact: worst case scenario. Right path corresponds to a weak impact.

Accordingly, the solution requires 3D analysis of the thermal/fluid/structure interaction in the supersonic flow. In addition the number of sensors available onboard is severely limited and the safe time window between the detectable onset of the fault and possible catastrophic failure is typically a few seconds.

To overcome these difficulties we use a combination of physics based analysis and high-fidelity modeling. The analysis is performed for the worst case scenario and divided in three steps. In the first step (Sec. II) the structural dynamics of the nozzle during the separation failure is analyzed using finite element model and the theory of shells. It is shown that the nozzle buckles as a result of the impact. At the second step (sec. III) the pressure and temperature loads on the walls of the deformed nozzle in the hot gas flow are estimated analytically and numerically. It is shown that the most plausible consequence of the nozzle buckling is melting and disintegration of the thin nozzle walls in the region of the maximum plastic strain. High-fidelity simulations are employed to estimate the reduction of the actual thrust and side loads induced by the fault. In Sec. IV, we use the results of the preceding analysis to suggest the FD&P system of the stage separation fault based on the TVC actuator measurements of the fault-induced torque. Finally, we provide the discussion of the results and outline future direction of research.

2. STRUCTUAL DYNAMICS

A typical geometry of a separation failure is sketched in the Figure 1. Fault induced by lateral velocity of the inter-stage results in a separation trajectory that crosses the nozzle. The greater is the lateral velocity the larger is the overlap of the inter-stage and he nozzle and more severe is the consequence of the impact. The goal of the FD&P system is to detect the impact, estimate its strength, and to
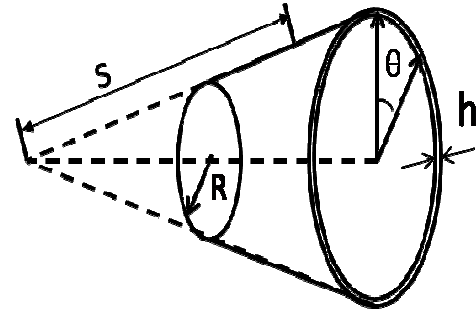

Figure 1 Sketch of the nozzle as a conical shell defined by the coordinates s and θ.

predict the fault-induced torque of the damaged nozzle after engine ignition.

is to detect the impact, estimate its strength, and to predict the fault-induced reduction of the actual thrust and side loads.

For the typical parameters of the nozzle extension of the liquid motor the nozzle dynamics under the interstage impact can be considered based on shell theory [1]. A simplified geometry of the nozzle extension corresponding to this model is shown in the Fig. 2. We consider dynamics of the second stage engine nozzle extension using Donnell's equation [1]

$$D\Delta^2 w + ch\frac{\partial w}{\partial t} + \rho h\frac{\partial^2 w}{\partial t^2} = f(t,s,\theta) + \frac{1}{R}\frac{\partial^2 N}{\partial x^2} \quad (1)$$

$$\frac{1}{G}\Delta^2 N + \frac{1}{R}\frac{\partial^2 w}{\partial x^2} = 0$$

where w transverse displacement, N- an Airy type of stress function, D and G are the bending and shear stiffness c - damping coefficient, h - thickness of the conical shell, R is the mean nozzle radius, $f(t,s,\theta)$ local external pressure acting on the nozzle from insterstage and

$$\Delta = \frac{\partial^2}{\partial s^2} + \frac{1}{s}\frac{\partial}{\partial s} + \frac{1}{s^2\sin^2\alpha}\frac{\partial^2}{\partial\theta^2}, \quad \nabla_R^2 = \frac{1}{s\tan\alpha}\frac{\partial^2}{\partial s^2},$$

are operators in cylindrical coordinate system, θ is the angular coordinate.

We consider boundary conditions for the trancated conical shell, short end of which is clamped and free large end is free. To find the eigenfunctions and eigenfrequencies of the problem we consider the next eigenvalue prolem

$$\begin{pmatrix} D\hat{a}(n) & -\hat{b} \\ \hat{b} & G^{-1}\hat{a}(n) \end{pmatrix}\begin{pmatrix} w(s) \\ F(s) \end{pmatrix} = \begin{pmatrix} h\rho\omega^2 \\ 0 \end{pmatrix}\begin{pmatrix} w(s) \\ F(s) \end{pmatrix} \quad (2)$$

2

where

$$\hat{a} = \left[\frac{d^4}{ds^4} + \frac{2}{s}\frac{d^3}{ds^3} - \frac{1+2n^2}{s}\frac{d^2}{ds^2} + \frac{1+2n^2}{s^2}\frac{d}{ds} - \frac{n^2(4-n^2)}{s^4} \right],$$

$$\hat{b} = \frac{1}{s\tan\alpha}\frac{d^2}{ds^2}.$$

The eigenfunctions $w_{mn}(s)$, $N_{mn}(s)$ satisfying Eq. (2), and natural frequencies ω_{mn} of the cone can be found out by Galerkin's or Rayleigh--Ritz methods. Expanding the radial displacement w and Airy function N in the series of the shallow shell eignemodes

$$w(t,s,\theta) = \sum_{mn} c_{mn}(t)w_{mn}(s)\cos(n\theta),$$

$$N(t,s,\theta) = \sum_{mn} d_{mn}(t)N_{mn}(s)\cos(n\theta)$$

where n is the number of waves in the circumferential direction and using the property that normal modes with different indexes are orthogonal we obtain equations governing the amplitudes c_{mn} as

$$\frac{\partial^2 c_{mn}}{\partial t^2} + 2\delta\frac{\partial c_{mn}}{\partial t} + (\omega^2_{mn})c_{mn} = f_{mn}(t) \qquad (3)$$

where $\delta = c/2\rho$,

$$f_{mn}(t) = \frac{1}{h\rho}\iint f(t,s,\theta)w_{mn}(s)\sin(n\theta)dsd\theta$$

Amplitutes d_{mn} differe form c_{mn} solution by the constant. Solution of the equation (3) with the intial condition

$$w_{mn}(0) = 0, \quad \dot{w}_{mn}(0) = 0$$

can be presented by Duhamel's integral [2]

$$c_{mn}(t) = \frac{\displaystyle\int_0^t f_{mn}(\tau)\sin\omega_{mn}(t-\tau)d\tau}{\omega_{mn}\|w_{mn}\|^2}$$

This approach makes it possible to calculate elastic stress-strain distribution in whole nozzle during the impact. For the impact time of the order of 50 msec we expect that the frequency range of the eigenmodes dominating the response dynamics will be limited by 10 Hz.

The linear elastic approach was justified by estimation of buckling stresses during impact. The external load $f(t,s,\theta)$ on the local surface can lead to sufficiently large stresses and nonlinear dynamics determined by plasticity.

The external buckling stresses corresponding to the lateral pressure of the conical shell was estimated by formula [1]

$$\sigma = \frac{\sqrt{6}\pi E}{9(1-\nu^2)^{3/4}}\frac{h}{L}\left(\frac{h}{R}\right)^{1/2} \approx E\left(\frac{h}{R}\right)^{3/2}. \qquad (4)$$

where E is the Young's modulus of the cone, L is the length of the cone which is of the same order with radius ($L{\sim}R$). Considering $E=2\times10^{11}$ Pa, $h/R\approx2\times10^{-3}$ we have the buckling pressure 2×10^7 Pa, which is of the same order, observed in the nozzle during impact simulations. This is why Finite Element model was developed.

To analyze response of the nozzle to the impact we build a finite element model of the nozzle extension in ABAQUS. Because the nozzle shell is much thinner then the impacting part the later is modeled as a rigid body. We fix the nozzle extension at its base and use a dynamic explicit mode with general contact properties to simulate the impact. Typical results of the simulations are shown in the Figure 3. It can be seen from the figure how the nozzle is damaged during the impact. One of the main conclusions of the simulations is that the nozzle buckles as a result of the impact. The buckling stresses found in the numerical simulations confirm the values obtained with analytical estimations above.

Next we estimate the impact-induced torque on the nozzle. The results are shown in the Figure 4 for three different values of the overlap of the nozzle extension with the impacting cylindrical shell at the initial moment of the impact.

It can be seen from figures that the strength of the impact can be inferred from the analysis of the torque signal and specifically from the amplitude of the first impulse. In addition the lateral relative velocity of the separation is usually associated with the malfunction of the accelerating/decelerating motors. As a result axial velocity is also affected by the fault and there is a fault-
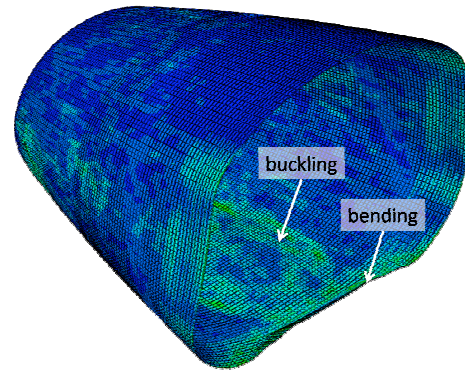

Figure 3 Results of the simulations of the impact. The bended and buckled areas of the nozzle are shown by the arrows.
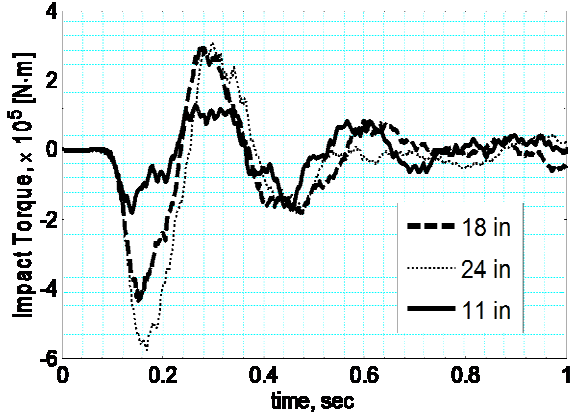
Figure 4. Impact-induced torque on the nozzle for three different overlaps of the nozzle extension with the impacting cylindrical shell at the initial time of the impact.
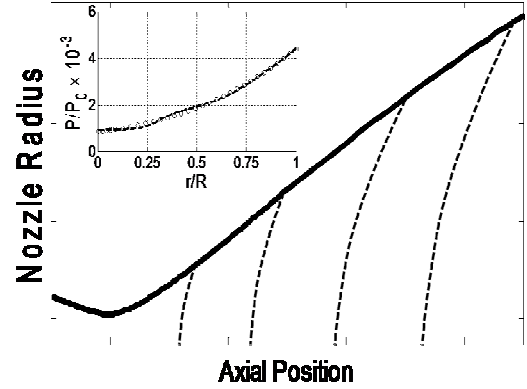

Figure 5. Radial pressure distribution in quasi-two-dimensional approximation is shown for four different locations along the nozzle axis. Radial pressure distribution (circles) as compared with the results of high-fidelity simulations (dashed line).

induced delay time between the separation initiation and the impact instant. The more sever is the fault the larger is the delay. Therefore correlation between the amplitude of the impact torque and the impact delay time can serve as an additional characteristic dynamical signature of the separation fault that helps to infer the fault induced damage.

Our analysis shows that the damage can be characterized by two key factors: (i) the area S of the dent and (ii) the angle of the bend. For the separation failure geometry shown in Figure 2 the area of the damage can be as large as 0.5 m^2 and the angle of the bending of the nozzle vary from 30 to 50 degrees. It will be shown in the following discussion that the structural stability of the nozzle and fault induced changes of the thrust are mainly determined by the area and angle of the bending.

3. TRANSIENT LOADS ON THE NOZZLE

To estimate further degradation of the damaged nozzle in the hot gas flow one has to determine pressure and temperature loads on the nozzle walls caused by the flow. To do so we use combination of high-fidelity simulations and analytical estimations. Analytical estimations are based on the analysis of the flow parameters at the nozzle surface in the presence of the dent. To determine transient parameters of the flow a quasi-two-dimensional model of the flow introduced. This model is verified by comparison with static high-fidelity simulations. The transient loads on the wall are then introduced into the finite element model of the nozzle to analyze coupled thermal-structural dynamics of the damaged nozzle in the hot gas flow.

3.1 Quasi-two-dimensional approximation

To estimate the pressure and temperature loads on the damaged nozzle a quasi-two-dimensional model of the transient flow is introduced as follows. Let us first

consider a one dimensional isentropic model of the nozzle flow for given transient time traces of the pressure $p_0(t)$, mass flow rate $J(t)$, and temperature $T_0(t)$ in the main combustion chamber. The exit pressure $p_{ex}(t)$ and temperature $T_{ex}(t)$ can be written in the form

$$T_{ex} = T_0\left(1 - \frac{(\gamma-1)}{2}M_{ex}^2\right), \quad p_{ex} = p_0\left(1 - \frac{(\gamma-1)}{2}M_{ex}^2\right)^{\frac{\gamma}{\gamma-1}}. \quad (5)$$

We note that the Mach number at the exit $M_{ex} = u_{ex}/c_0$ does not depend on the flow variations and is determined by the nozzle geometry and the specific heat ratio $\gamma = c_p/c_v$

$$M_{ex}\left(1 - \frac{(\gamma-1)}{2}M_{ex}^2\right)^{\frac{1}{\gamma-1}} = \frac{S_t}{\Gamma S_{ex}}, \quad \Gamma = \left(\frac{\gamma+1}{2}\right)^{\frac{\gamma+1}{2(\gamma-1)}}, \quad (6)$$

where S_t is the nozzle throat area and S_{ex} is the nozzle exit area. Thus time variation of the thrust is completely determined by the time variation of the chamber pressure according to the following expression

$$F_{th}(t) = \frac{\gamma}{\Gamma}p_0(t)S_tM_{ex}. \quad (7)$$

To determine pressure and temperature loads on the nozzle wall we use the results of static high-fidelity simulations. The radial distribution of pressure obtained in high-fidelity simulations is shown in the insert of Figure 5 by open circles. We next require that: (i) for every location along the nozzle axis the mean value of the radial pressure distribution coincides with the values obtained using one-dimensional model (5); (ii) the wall pressure coincides with the results of the high-fidelity simulations; and (iii) the values of the vacuum thrust calculated using Eq. (7) correspond to the vacuum thrust obtained by integrating pressure on the nozzle walls.
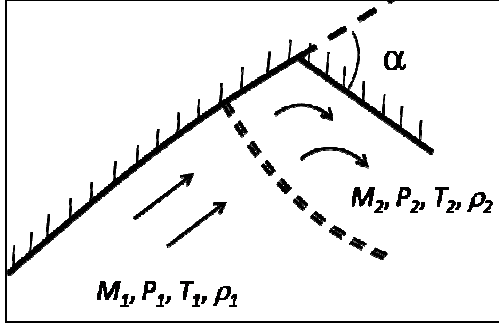
Figure 6. Oblique shock wave with deflection angle α near the bending corner of the damaged area is shown by the dashed bended lines. Parameters of the incident and aftershock flaws are indicated by sub-indexes 1 and 2 respectively.

These conditions can be satisfied using polynomial fit of the high-fidelity radial pressure distribution and requiring that mean value of this polynomial approximation is given by Eq. (5). A quasi-two dimensional distribution of pressure in the nozzle obtained in such approximation is shown in the Figure 5. Similarly we obtain quasi-two-dimensional distribution of the flow temperature. The advantage of such approximation is that it allows us to obtain accurate representation of the transient nozzle flow parameters near the nozzle wall at the location of the damage.

Next, we apply this approximation to analyze the shock structure near the damaged wall and to estimate the pressure and temperature loads on the damaged wall induced by the aftershock flow.

3.2 Temperature and pressure loads

To estimate temperature and pressure loads on the wall we recall that whenever a supersonic flow is "turned into itself" as shown in Figure 6 an oblique shock wave will occur (Shapiro, 1953; Andreson, 2001). The analysis shows that for deflection angles α as large as 50 and relevant gas parameters the flow at the corner will correspond to the detached curved shock wave as shown in Figure. Accordingly, estimation from above for the pressure and temperature loads on the damaged wall can be performed using equations for the normal shock wave in the form

$$M_2^2 = \frac{1+\left[(\gamma+1)/2\right]M_1^2}{\gamma M_1^2 - (\gamma-1)/2},$$

$$\frac{p_2}{p_1} = 1 + \frac{2\gamma}{(\gamma+1)}\left(M_1^2 - 1\right), \qquad (8)$$

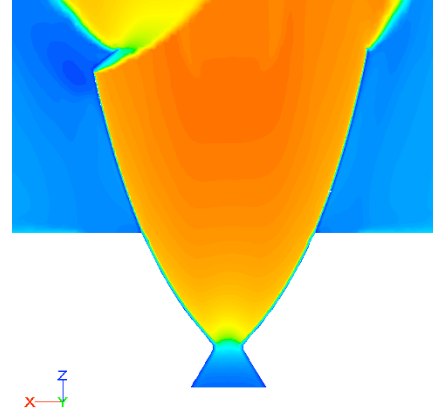$$\frac{T_2}{T_1} = \frac{1+\left[(\gamma-1)/2\right]M_1^2}{1+\left[(\gamma-1)/2\right]M_2^2}.$$

Figure 7. Distribution of the velocity of the gas flow in the damaged nozzle. The damaged area and the formation of the detached oblique shock wave can be seen in the left upper corner of the nozzle.

To estimate temperature and pressure loads from below we use the smallest deflection angle $\alpha = 30$ of the damaged area obtained in structural dynamics simulations, substitute in the first Eq. (8) the values of the Mach numbers M_1 and M_2 with the values of Mach numbers normal to the shock, and find the shock wave angle β by solving the equation

$$\tan\alpha = 2\cot\beta\frac{M_1^2\sin^2\beta - 1}{M_1^2(\gamma+\cos 2\beta)+2}. \qquad (9)$$

The resulting pressure loads on the damaged wall range from approximately 1 atm (weak oblique shock with deflection angle $\alpha = 30$) to several atmospheres (normal detached shock). The corresponding temperature on the wall varies from 2200 K to 3700 K, which exceeds the melting temperature $T_{mel} \approx 2150$K.

This analytical estimation were confirmed by the high-fidelity simulations of the gas flow in the damaged nozzle using FLUENT. An example of the velocity distribution obtained in these simulations is shown in Figure 7. The formation of the detached oblique shock wave can be clearly seen near the dent corner of the nozzle.

Note that the obtained pressure and temperature loads may result in yielding and melting away of the nozzle dent as will be discussed in the following section. We now estimate the time scale required for yielding, melting, and burning through the damaged area of the nozzle.

3.3 Fault-induced transient torque

It was shown in the previous section that the temperature loads on the damaged wall exceed the melting temperature. Accordingly, the transient dynamics of the effect of the flow on the damaged wall will be mainly determined by the time required to heat the wall to the melting temperature. Simultaneously with nozzle heating the rise of the pressure load during the engine ignition
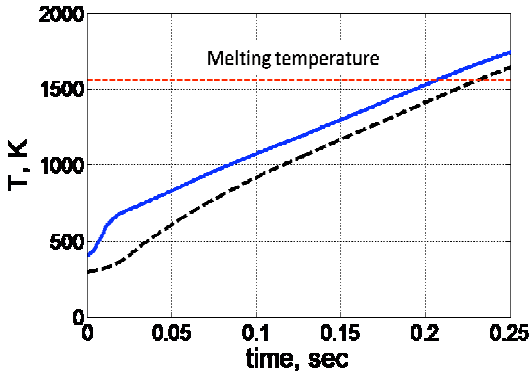
5

Figure 8. Dynamics of the temperature of the internal (blue solid line) and external (black dashed line) surfaces of the damaged nozzle. Red horizontal line shows melting temperature on the nozzle material.

transient will exceed yielding limit required for reversed buckling just before the nozzle will begin to melt.

To estimate the characteristic time scale of the corresponding dynamics of heating and buckling of the damaged nozzle, we use time traces of the ignition transient for the temperature and pressure reported by (Wang and Guidos, 2009). According to their results the pressure and temperature jump of the nozzle flow occurs 1.7 sec after ignition when the nozzle is uniformly filled with the supersonic flow. The subsequent rise of the flow parameters to the nominal steady values occurs on the time scales from 0.5 to 1.0 sec with the fastest rising time ($\approx$ 0.5 sec) corresponding to the temperature change.

We use ABAQUS to integrate equation of structural dynamics of the damaged nozzle under transient pressure load coupled with the solution of the heat equation for the
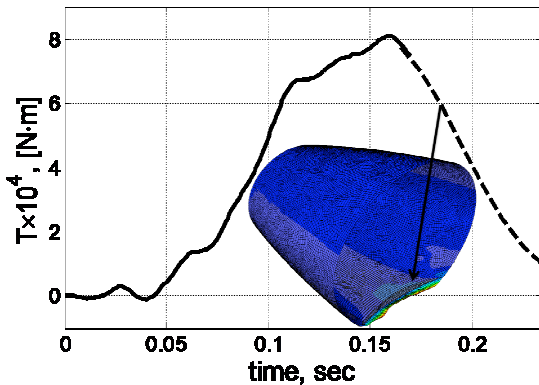

Figure 9. Torque induced by the transient dynamics of the aftershock temperature and pressure loads on the damaged nozzle area $S \approx 0.15$ m^2. The inset shows the change in the shape of the damaged area 0.18 sec after the pressure jump. The initial shape is shown by the gray contour; the modified shape is shown in colored contour.

wall temperature T where boundary conditions correspond to the heat flux from the gas flow to the internal surface of the nozzle with the heat transfer coefficient η and zero flux on the external surface of the nozzle.

The temperature dynamics are shown in Figure 8. It can be seen from the figure that the temperature of the external side of the thin nozzle walls approaches melting temperature T_{mel} in approximately 0.23 sec.

To estimate the characteristic time of the heating of the nozzle wall analytically we use Bartz' approximation (Bartz, 1965; Incropera and DeWitt, 2002) for the heat transfer from the gas flow to the nozzle wall. Since the nozzle wall is very thin the analysis is performed in 1D using the following equation for the dynamics of the nozzle temperature $T(x,t)$

$$\begin{cases} T_t = \dfrac{\kappa}{C_{met}\rho_{met}} T_{xx}, & x_1 > x > x_0, \quad t > t_0 \\[2mm] -\kappa \dfrac{\partial T(x,t)}{\partial x}\bigg|_{x=x_0} = \eta\left(T_{inf} - T\right)\big|_{x=x_0} \\[2mm] -\kappa \dfrac{\partial T(x,t)}{\partial x}\bigg|_{x=x_1} = 0, \quad T(x,t_0) = T_0, \end{cases} \quad (10)$$

Here internal surface is situated at $x = x_0$ and external surface is situated at $x = x_1$. The solution of this equation gives an estimate for the characteristic melting time approximately 0.2 sec in good agreement with numerical results.

However, even before the melting begins the pressure load on the wall exceeds the critical value for reversed buckling. Indeed, the critical stress can be estimated as $\sigma = pS/h^2$ where p is the aftershock pressure, S is the damaged area, and h is the nozzle wall thickness. For $h \approx$ 5 mm, $S \approx 0.5$ m^2, and given pressure transient time-traces the critical pressure $p \approx 7 \times 10^4$ Pa is reached in approximately 0.16 sec after the pressure jump (i.e. approximately 1.85 sec after engine ignition). At this moment the reversed buckling of the damaged area of the nozzle is initiated by the pressure loads induced by the nozzle flow. The damaged nozzle wall will begin to melt down approximately 40 msec later. So in approximately 2 sec after the engine ignition the damaged area of the nozzle will burned through by the gas flow.

To analyze this sequence of events in more details we solve numerically the coupled temperature-displacement problem in ABAQUS for the relevant parameters of the flow (Hill and Peterson, 1992). The results of these simulations are shown in Figure 9. The analysis reveals that the reversed buckling begins at approximately 0.16 sec after the pressure jump and the dent is completely buckled back 0.25 sec after the pressure jump.

Thus our analysis shows that under plume loading the dent causes a reaction torque and temperature load on the
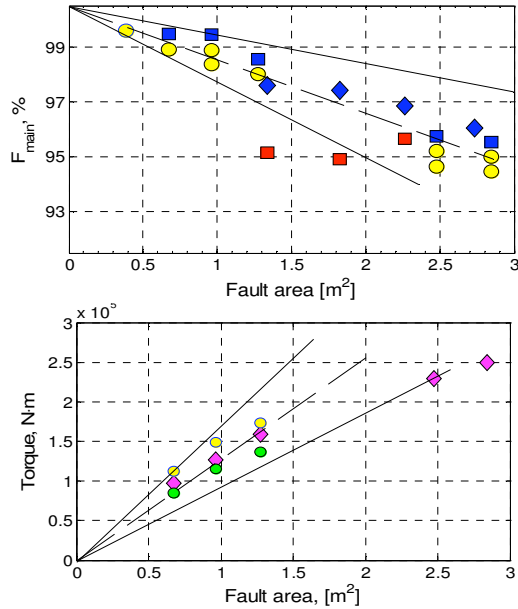
Figure 11. Transient torque induced by impact and the flow.

Figure 10. (top) The reduction of the actual thrust in the notched nozzle as function of the notch area S_n. Different colors correspond to different meshes of the model. The eye guiding lines approximate the mean value (dashed lines) and the error of estimation (solid lines). (bottom) The side load developed in the damaged nozzle as a function of the notch area. The results of the numerical calculations are shown by magenta rhombus, the green and yellow circles show results of analytical estimations.

nozzle until the damaged area yields and melts away, leaving a notch in the nozzle wall.

4. QUASI-STEADY THRUST

Finally we estimate reduction of the actual thrust and the side load in the notched nozzle in quasi-steady regime. The results of the numerical simulations for different values of the S_n are shown Figure 10 (top). The thrust was calculated as a product of the velocity and the mass flow rate the at the nozzle exit surface. The analysis shows that the reduction of the actual thrust and the side load caused by the notch are both linearly proportional to the notch area S_n.

The results of the numerical calculation of the fault-induced torque are shown in Figure 10 (bottom). together with the results of analytical estimations. The later estimations were obtained in the point force approximation. It was assumed the force on the wall in radial direction is compensated everywhere except at the notch area and symmetrically situated undamaged area of the nozzle S_{n0}. The force on the notch was equal to zero and the force on the undamaged area was calculated as a point force and equal to the integral of the nominal pressure on the nozzle wall over S_{n0}. The estimations
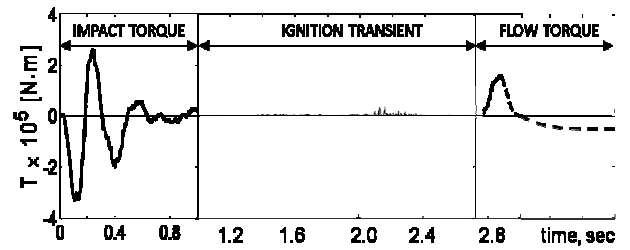
shown by the green circler correspond to the assumption that there is no asymmetry in the axial load. The estimations shown by the yellow circles take into account the asymmetry of the load in axial direction. The results of the analytical estimations are in a good agreement with the results of numerical simulations.

5. CONCLUSIONS

The analysis of the torque induced by the impact and by the ignition transient loads on the damaged nozzle reported above allows one to build the FD&P system for in-flight detection of the stage separation failure and prediction of the fault induced thrust.

As it was shown in Sec. II the impact induced torque provides a convenient tool for detection of separation failure and inferring the size of damage via measurements of the amplitude of the first peak of the impact torque. In addition, correlation between the amplitude of the torque and the time delay between the separation ignition and the impact signal can be used to improve the accuracy of the detection algorithm. It was shown further in Sec. III that fault induced damage of the nozzle will result in significant ignition transient torque imposed by the flow on the buckled area of the nozzle surface. The value and sign of this torque are strongly correlated with the strength of the impact. In particular, flow will induce torque in the same plane of separation in the opposite direction compared to the impact induced torque. It was also shown in Sec. III that the heat and pressure loads generated by the oblique shock wave near the dent corner of the damaged nozzle will result in reverse buckling of the damaged area with its subsequent melting and disintegration. The time scale of this process was estimated to be approximately 0.23 sec. As a result the torque induced by the flow will change its sign one more time and will approach quasi-equilibrium value proportional to the damaged area. For convenience we have summarized the torque time-traces at different stages of the separation failure in Figure 11. The in-flight analysis of these time-traces can be conveniently performed within a Bayesian inferential framework similar to the one introduced in our earlier work (Luchinsky, 2009; Osipov, 2007) for the in-flight

diagnostic and prognostic of the case breach fault in Solid rocket motor. The corresponding work is currently in progress.

NOMENCLATURE

ρ	gas density
p	gas pressure
T	gas temperature
u	gas velocity
c	sound velocity
h	thickness of the nozzle wall
M	Mach number, $M = u/c$, $M_0 = u/c_0$
C_V	specific heat for the constant volume
C_P	specific heat for the constant pressure
γ	ration of specific heats; $\gamma = C_p/C_V$
R	nozzle radius
A	cross-sectional area of the nozzle
S	area of the damaged part of the nozzle
F_{th}	thrust produced by gas flow
F_S	side thrust
j	mass flow density [$j = u\rho$]
η	heat transfer coefficient
Q	heat flow from the gas to a hole wall
T_{mel}	melting temperature point
T_b	temperature of metal surface burning
C_{met}	specific heat of case metal
ρ_{met}	density of case metal
κ	thermal conductivity
	dynamical viscosity of hot gas
w	vertical deflection of the nozzle surface
D	bending stiffness
G	shear stiffness
R	nozzle radius
h	nozzle wall thickness
s, θ	nozzle surface coordinates
N	Airy type of stress function
α	deflection angle
β	shock wave angle

Subscripts:

in	initial states
ex	parameters in the nozzle exit
t	parameters in the nozzle throat
0	parameters in the chamber

REFERENCES

ABAQUS http://www.simulia.com/

J. D. Andreson. (2001). *Fundamentals of Aerodynamics*, New York: McGraw-Hill Higher Education.

D.R. Bartz. (1965), *Heat Transfer from Rapidly and from Heated Air*, in Advances in Heat Transfer, vol. 2, Hartnett, J. P. , and Irvine, T. F. Jr., eds., New York: Academic Press.

Futron Corporation, Design Reliability Comparison for SpaceX Falcon Vehicles, http://www.spacex.com/ (2004).

FLUENT www.ansys.com/

P. Hill and C. Peterson (1992), *Mechanics and Thermodynamics of Propulsion,* 2-rd ed., Addison-Wesley Publishing Company, Inc. New York.

F.P. Incropera and D. P. DeWitt (2002), *Introduction to Heat Transfer*, John Wiley & Sons, NY,

D.G. Luchinsky, V.V. Osipov, V.N. Smelyanskiy, D.A. Timucin, S. Uckun, B. Hayashida, M. Watson, J. McMillin, D. Shook, M. Johnson, S. Hyde. (2009, March), "Fault Diagnostics and Prognostics for Large Segmented SRMs", *in Proceeding of 2009 IEEE Aerospace Conference,* Big Sky, Montana.

V.V. Osipov, D.G. Luchinsky, V.N. Smelyanskiy, C. Kiris, D.A. Timucin, S.H. Lee. (2007). In-Flight Failure Decision and Prognostic for the Solid Rocket Buster, *in Proceeding of AIAA-2007-5823, 43rd AIAA/ASME/SAE/ ASEE Joint Propulsion Conference and Exhibit,* Cincinnati, OH.

C. Seife, "SPACE SHUTTLE: Columbia Disaster Underscores the Risky Nature of Risk Analysis", *Science* 14 February 2003: Vol. 299. no. 5609, pp. 1001 – 1002.

A.H. Shapiro. (1953). "The Dynamics and Thermodynamics of Compressible Fluid Flow", Ronald Press, NY, vol. I ,

V.N. Smelyanskiy, D.G. Luchinsky, V.V. Osipov, D.A. Timuchin, S.Uckun. (2008, July*)*, "Development of an on-board failure diagnostics and prognostics system for Solid Rocket Booster", *in Proceeding of 44rd AIAA/ASME/SAE/ASEE Joint Propulsion Conference & Exhibit, Hartford, CT.*

T.-S. Wang and M. Guidos (2009). Transient Three-Dimensional Side-Load Analysis of a Film-Cooled Nozzle, *Journal of Prop and Power,* Vol. 25, no. 6, 1272-1280.

Dr. **Dmitry G. Luchinsky** is a senior research scientist in MCT Inc. He obtained his MSc and PhD in physics in Moscow working on nonlinear optics of semiconductors. He is an author of more than 100 publications. He has been on a number of occasions a Royal Society Visiting Fellow and a NASA visiting scientist. He worked as a senior scientific researcher in VNII for Metrological Service (Moscow, Russia) and as a Senior Research Fellow in Lancaster University (Lancaster, UK). His research interests include nonlinear optics, stochastic and chaotic nonlinear dynamics, dynamical inference, fluid dynamics, ionic motion. His

research is currently focused on theory and CFD of gas dynamics and fluid structure interaction in SRBs.

Dr. **Viatcheslav (Slava) V. Osipov** is a leading research scientist in MCT working at NASA Research Centre on nonlinear spatial extended systems far from equilibrium with application to semiconductor physics and hydrodynamics. Slava Osipov received MS, Engineer-Physicist followed by Ph.D. and Sci. Doc. in Physics of non-equilibrium systems" (1975) from Moscow Institute of Physics and Technology (MIPT) for the study of self-organization phenomena in physical, chemical, and biological system. He was a professor in MIPT and a science-director of the Department of Fundamental Research and Theoretical Physics in Russian State Science Center "ORION", Moscow, Russia. Dr. Osipov has published 4 books and more than 250 science articles in the leading physical journals. He have worked a research professor in scientific laboratories of different countries, including in Consejo Superior de Investigaciones Cientificas, Madrid, Spain, in University of New South Wales (UNSW), Sydney, Australia, and in Hewlett-Packard Labs, CA, USA.

Dr. **Vadim N Smelyanskiy** leads the physics modeling group in Computation Science Division at NASA Ames Research Center. He has obtained his BS, MS, and PhD in Institute of Semiconductors (Kiev, Ukraine). He has worked as a consultant and research Scientist in Los Alamos National Lab., Departments of Physics in Ann Arbor, MSU, and Princeton. Currently his research interest include nonlinear dynamics, statistical mechanics, Bayesian Statistics, nonlinear modeling, computer vision, quantum, computer, fluid dynamics of solid rocket motors, nonlinear dynamics of CMG.